SCIENCE CHINA
Earth Sciences

• RESEARCH PAPER •

doi: 10.1007/s11430-012-4383-6

Three-dimensional MHD simulation of the lunar wake

XIE LiangHai[1,2] , LI Lei[1*], ZHANG YiTeng[1] & Darren Lee De ZEEUW[3]

[1] *Center for Space Science and Applied Research, Chinese Academy of Sciences, Beijing 100190, China;*
[2] *Graduate University of Chinese Academy of Sciences, Beijing 100049, China;*
[3] *Center for Space Environment Modeling, University of Michigan, Ann Arbor, Michigan 48109-2143, USA*

Received September 26, 2011; accepted February 15, 2012

We study the interaction between the Moon and the solar wind through a three-dimensional MHD simulation. Three cases have been discussed in which the interplanetary magnetic field lies at 90°, 180°, and 135° to the solar wind flow, respectively. A wake with low density and low pressure can always be formed behind the Moon. The plasma temperature and magnetic field are enhanced in the central wake, but the field strength is reduced in the surrounding region. A Mach cone is formed by rarefaction waves emanating from the limb. These rarefaction waves propagate via the fast magnetosonic mode with different velocities in different directions relative to the magnetic field. When the interplanetary magnetic field is not parallel to the solar wind flow, the wake shows some asymmetries, with an acceleration region turning up at the center. Finally, the results are compared with the observations by WIND spacecraft. Our calculations agree reasonably well with the observed values.

lunar wake, MHD simulation, solar wind

Citation: Xie L H, Li L, Zhang Y T, et al. Three-dimensional MHD simulation of the lunar wake. Sci China Earth Sci, 2012, doi: 10.1007/s11430-012-4383-6

Observations by Explorer 35 show that the Moon does not have an atmosphere and a significant intrinsic magnetic field, and that the conductivity of the lunar body is also very low. The Moon can be treated as an insulated sphere when it interacts with the solar wind, and thus the interplanetary magnetic field (IMF) can pass through it nearly unperturbedly. The solar wind plasma is absorbed for the most part on the dayside when it comes into contact with the lunar surface, leaving a plasma void on the night side [1] and finally resulting in a wake structure behind the Moon. As the system attempts to restore pressure balance, the magnetic field exhibits a corresponding gradual increase towards the center of the wake [2]. Due to the small scale of the moon and large gyroradius of solar wind particles, the wake is quite kinetic in nature. Observations by WIND spacecraft showed more characteristics of the lunar wake. For example, two distinct proton distributions were simultaneously detected, one convecting with a speed slightly faster than the ambient solar wind and the other convecting slightly slower; and the electron temperature increased in the wake by a factor of about four, while the ion temperature remained fairly constant [3].

As for modeling the Moon-solar wind interaction, there are three main ways: magnetohydrodynamic (MHD) models, fully kinetic models, and hybrid models. Spreiter et al. [4] were the first to use an MHD approximation to discuss the large scale characteristics of the lunar wake. They obtained the structure of the lunar wake, the approximate boundary of the void region and the corresponding density, pressure and magnetic field distributions. However, the position of the void boundary is artificial, and thus the results are not self consistent. A numerical simulation by Cui et al. [5] with the ideal MHD equations could get the density, velocity, pressure and magnetic field distributions in the whole sim-

*Corresponding author (email: lil@nssc.ac.cn)

ulation region self consistently. But as a two-dimensional (2-D) model, with the first-order finite differential scheme used, it is difficult to reveal the details of the interaction. To better understand the kinetic processes in the lunar plasma environment, some fully kinetic models based on particle in cell (PIC) scheme have been developed, such as one-dimensional (1-D) self-consistent simulation studies using an electrostatic approximation [6, 7] and 2-D electromagnetic simulations [8]. They do well in describing the WIND observations of counter streaming ion beams and all kinds of electrostatic instabilities. Nevertheless, it is not easy to do a three-dimensional (3-D) kinetic simulation with current numerical and computational means. In addition, fully kinetic models are focused on electrostatic, high-frequency processes [9]. These limitations have been alleviated in so-called hybrid models, which treat the ions as particles and the electrons as massless charge neutralizing fluid [10, 11]. The hybrid models obtain full dimensional features of the lunar wake. Some kinetic effects are also found, such as non-Maxwellian plasma beams [10], and density and magnetic field variations in the far wake which may be caused by ion beam instability [11]. However, the numerical method for a 3-D self consistent hybrid model with high spatial resolution is also immature and usually needs some simplifications. The model by Kallio et al. [10] uses a fairly coarse grid in a small region, and does not handle the wake region in a self consistent way (the electric field is specified in that region). The model by Holmström et al. [11] is self consistent with higher spatial resolution and most of the results are also in accord with most of the observations by WIND spacecraft. But it has no simulation data in the central wake since the density in this area is too low. Moreover, the electron temperature decreases in the wake, which is contrary to the WIND observations [3], for it just uses the adiabatic equation $(p_e / \rho_e^{\gamma}) = \text{Constant}$ to determine electron pressure [11].

Given that the gyroradius of the solar wind proton here is about 1/30 of the lunar radius, it is reasonable to make a fluid assumption [4]. Generally speaking, the MHD model has its particular advantage in numerical methods when studying the large scale characteristics of the lunar wake. In this paper, we present a 3-D MHD model with high spatial resolution to describe the Moon-solar wind interaction. We discuss three cases in which the IMF lies at 90°, 180°, and 135° with respect to the solar wind flow, respectively. We also compare the results with the observations by WIND.

1 MHD simulation

Suppose the Moon is an insulated sphere with no atmosphere and intrinsic magnetic fields, and the physical variables of solar wind plasma can be described by ideal MHD equations as follows:

$$\frac{\partial \rho}{\partial t} + \nabla \cdot (\rho \boldsymbol{u}) = 0, \tag{1}$$

$$\frac{\partial \rho \boldsymbol{u}}{\partial t} + \nabla \cdot (\rho \boldsymbol{u}\boldsymbol{u}) + \nabla p - \boldsymbol{j} \times \boldsymbol{B} = 0, \tag{2}$$

$$\frac{\partial E}{\partial t} + \nabla \cdot \left[(e + p)\boldsymbol{u} + \frac{(\boldsymbol{B} \times \boldsymbol{u}) \times \boldsymbol{B}}{\mu_0} \right] = 0, \tag{3}$$

$$\frac{\partial \boldsymbol{B}}{\partial t} + \nabla \times (\boldsymbol{B} \times \boldsymbol{u}) = 0, \tag{4}$$

$$\nabla \times \boldsymbol{B} = \mu_0 \boldsymbol{j}, \tag{5}$$

$$\nabla \cdot \boldsymbol{B} = 0, \tag{6}$$

where ρ, $\boldsymbol{u}$, p, $\boldsymbol{B}$ and $\boldsymbol{j}$ are the density, the bulk velocity, the thermal pressure, the magnetic field and the electrical current density of the solar plasma, respectively. $E = p/(\gamma - 1) + \rho u^2/2 + B^2/2\mu_0$ is the total energy density, where γ is the ratio of specific heats and it can be set to 5/3 here. We assume the solar plasma can be regarded as ideal gas, then $p=nkT$ (where k is Boltzmann's constant, T is the plasma temperature and n is the plasma number density). $e = p/(\gamma - 1) + \rho u^2/2$ is the sum of the internal energy density and the kinetic energy density.

We use the Space Weather Modeling Framework (SWMF) [12], developed by the Center for Space Environment Modeling (CSEM) at the University of Michigan, to do such a simulation with a user-defined function to solve the boundary conditions. We choose a spherical grid with some local mesh refinements to define the grid mesh positions, whereas the physical variables are still expressed in a Cartesian coordinate system, as shown in Figure 1. The Cartesian coordinate system is centered at the Moon, with the x-axis directing toward the Sun, so the solar wind flows opposite to the x-axis. The y-axis is in the plane of x-axis intersecting with IMF, and points to the dusk side of the Moon. The z-axis completes the right handed coordinate system. We use the two-state HLL solver proposed by Linde [13] to solve Riemann problems and the explicit two-stage Runge-Kutta time stepping scheme. In this way, we can obtain a simulation solution with second order accuracy both in space and in time.

The extent of the simulation domain is x=[−24, 8]R_L, y=[−16, 16]R_L and z=[−16, 16]R_L, where R_L is the lunar radius, and R_L= 1738 km. The solar wind conditions are initialized by typical parameters at 1 AU [14]. The solar wind velocity is 461 km/s and in $-x$-direction, the number density is 7 cm^{-3}, the IMF is in xy-plane with a magnitude of 7 nT and the plasma temperature is T=2.5×10^5 K ($T=T_e+T_p$, where the electron temperature T_e is 1.4×10^5 K and the ion temperature T_p is 1.2×10^5 K). We use an absorbing boundary condition on the dayside, which means all

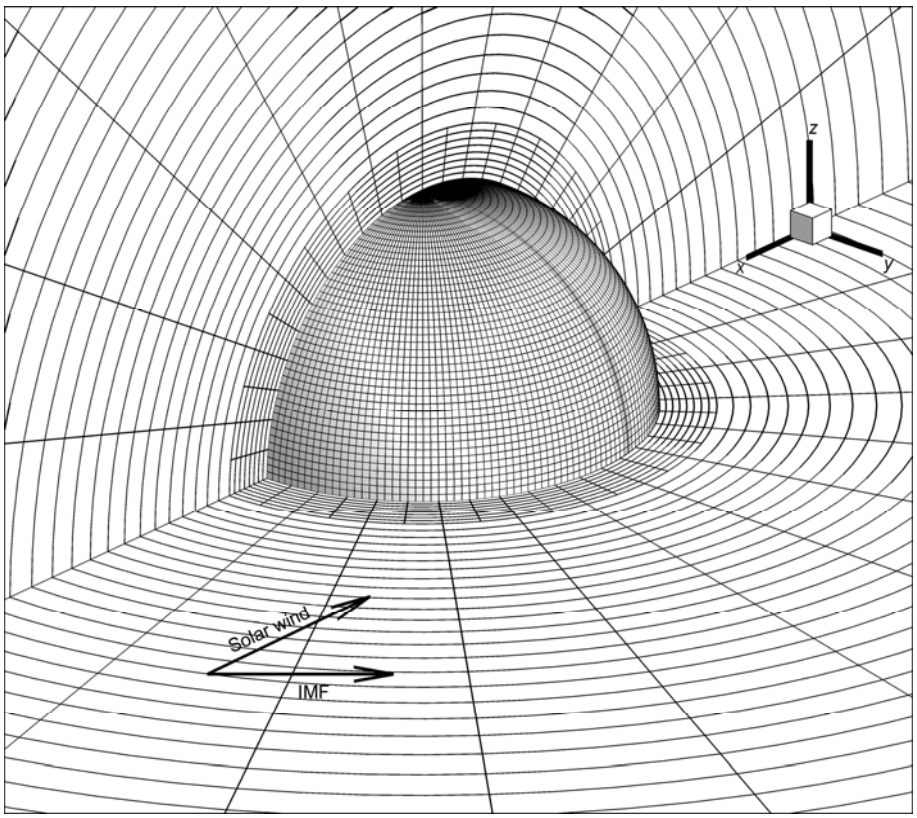

Figure 1 The grid and the coordinate system for simulation. The sphere at the origin indicates the Moon; the cuts are in the planes of y=0 and z=0.

the variables of the solar wind can pass the lunar surface freely. While on the night side, variables conform to the absorbing boundary condition except the normal velocity, which accords with a reflecting boundary condition.

2 Results and discussion

2.1 IMF perpendicular to the solar wind velocity (90°)

In this case, the IMF is in y-direction. Because of the absorption of solar wind on the dayside, a wake with low density and low pressure can be formed behind the Moon. As shown in Figure 2(1a), the plasma number density falls below 1.0 cm^{-3} at about x=−5R_L. Immediately surrounding the central wake is the expansion region with reduced field as reported by Ness et al. [2] and Halekas et al. [15]. The wake is gradually refilled by solar wind plasma mainly along the field lines (see Figure 3(1b)), due to the gradient in the thermal pressure. Plasma refilling from all directions will meet at the center of the wake and cause pressure increase there (see Figure 2(3a)) and the temperature is enhanced accordingly through adiabatic compression, which can be seen in Figure 2(5a), 2(5b), and 2(5c). In the x-direction, the gradient prevents the plasma flowing away from the wake. According to frozen-in-flux theorem, motions transverse to the field carry the field with them. Such a hindrance can drag the magnetic field lines and cause bending in the x-direction (see Figure 3(1a)). Bending of the magnetic field line creates a $\boldsymbol{j}\times\boldsymbol{B}$ force pointing along the $-x$-direction. The force is biggest at the center of the wake, in a narrow belt extending up to the polar regions (Figure 3(1a)), where it can speed up the solar wind plasma, and finally results in an acceleration region (see Figure 2(4a) and 2(4b)) in the wake just behind the Moon. As the energy in the magnetic field is converted into the kinetic energy, the field strength is relatively lower in the acceleration region (see Figure 2(2a), 2(2b)). On the other hand, the thermal pressure gradient also pushes some solar wind plasma to enter the wake perpendicular to magnetic field lines (see Figure 3(1c)), causing bending of the magnetic field lines in the z-direction. Similarly, a force pointing to the z-direction in the $z > 0$ area and a force pointing to the $-z$-direction in the $z < 0$ area are produced, which can hinder further wake refilling in the z-direction and then cause an asymmetry of streamlines in the y and z directions (see Figure 3(1b) and 3(1c)).

As the plasma refills the wake, a system of diamagnetic currents is formed by the pressure gradient across the wake boundary, $J=(B\times\nabla p)/B^2$, which produces a reduction in field strength in the expansion region, and an increase in field strength in the central wake [2, 16, 17]. The diamagnetic current system is asymmetric in this case, since the pressure gradient points outward; J is larger in the region where B is

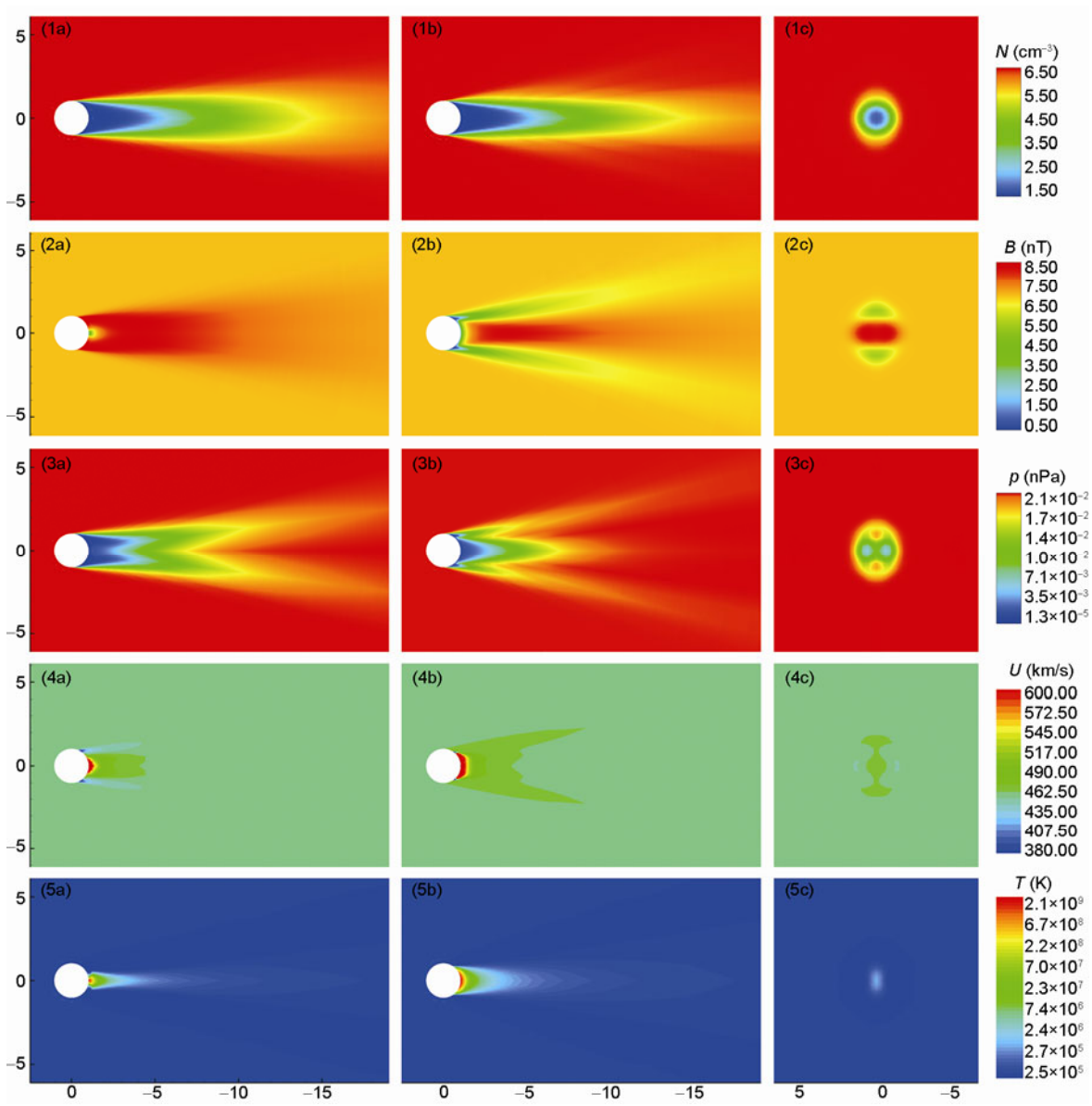

Figure 2 The simulation results when IMF is perpendicular to the solar wind. The columns from left to right are cuts in the planes z=0, y=0 and x=–4R_L. The rows from top to bottom represent the magnitudes of the number density, magnetic field, pressure, velocity and temperature of solar plasma, respectively.

quasi-perpendicular to ∇p than in the region where B is quasi-parallel to ∇p. The diamagnetic current is strongest in the polar region, where it produces the biggest disturbance in the magnetic field, and leads to a great decrease in the expansion region, as we can see from Figure 2(2b) and 2(2c).

According to the initial solar wind conditions, the acoustic wave velocity is $C_s = \sqrt{\gamma kT/m_i} \approx 58.6$ km/s, the Alfven velocity is $V_A = \sqrt{B^2/\mu_0\rho} \approx 57.8$ km/s,, and the fast magnetosonic wave velocity is $\sqrt{C_s^2 + V_A^2} \approx 82.3$ km/s. All of them are far less than the velocity of the solar wind, 461 km/s. The disturbances of the Moon on the supersonic solar wind are limited in a region called Mach cone, as shown by density, magnetic field, and pressure in Figure 2. The Mach cone is formed by rarefaction waves traveling outward from the limb with a cone angle of about 10.0° in the y=0 plane, and 7.5° in the z=0 plane. From the cone angle α=sin^{-1} (a/u)(where α is the cone angle, a is the velocity of disturbance propagation, and u is the velocity of the flow relative to the obstacle), it seems the rarefaction waves propagate via the fast magnetosonic mode, with sound speed C_s along y-direction, and fast magnetosonic wave speed $\sqrt{C_s^2 + V_A^2}$ along z-direction, due to the velocity

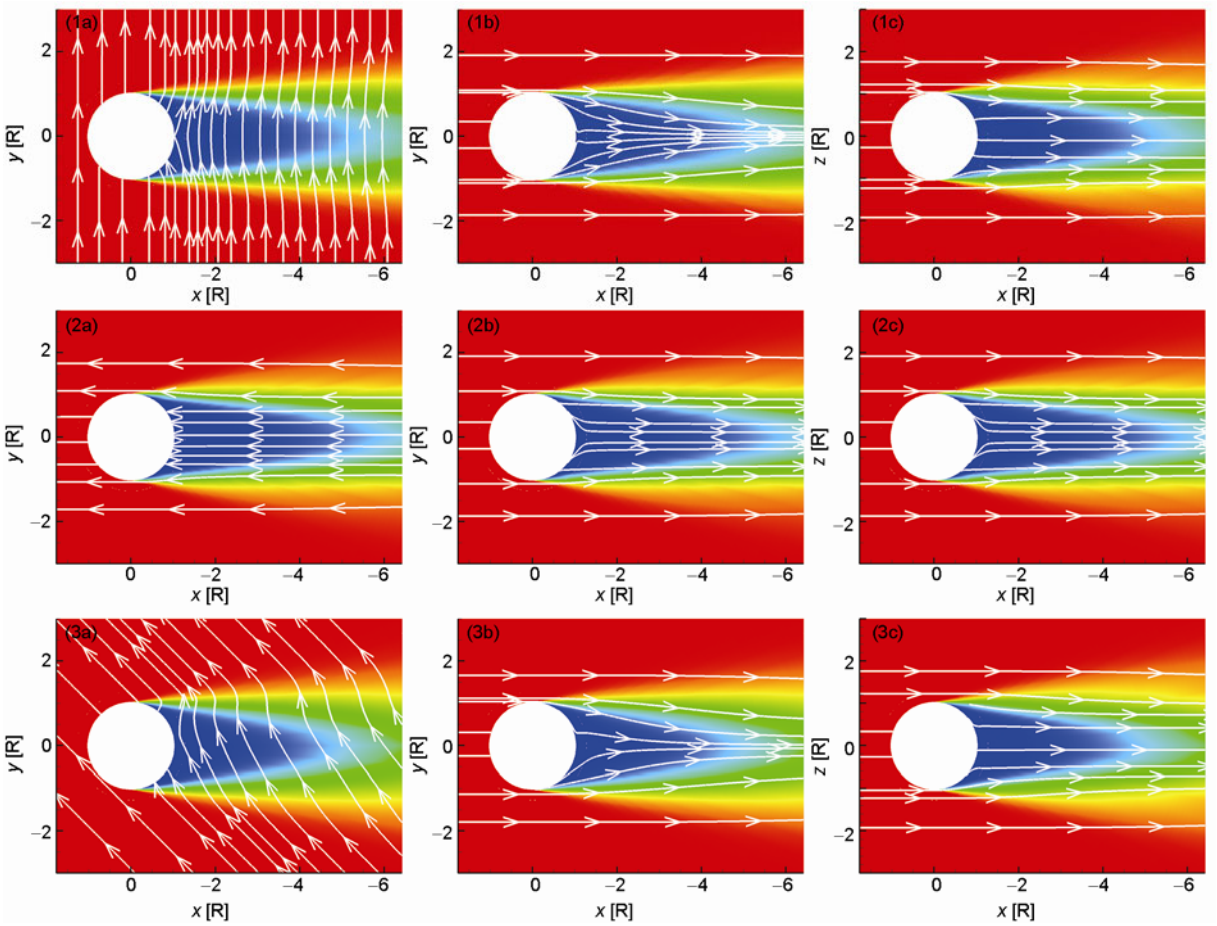

Figure 3 The magnetic field lines and streamlines. The left column represents the magnetic field lines in the *xy*-plane, the central column represents the streamlines in the *xy*-plane, and the right column represents the streamlines in the *xz*-plane. The contour images on the background represent the solar plasma number density. The rows from top to bottom represent the cases in which the IMF lies at 90°, 180°, and 145° to the solar wind flow, respectively.

anisotropy of the fast magnetosonic wave.

2.2 IMF anti-parallel to the solar wind velocity (180°)

Similar to the case when IMF is perpendicular to the solar wind velocity, a wake with low density and low pressure is formed behind the moon. The plasma flows along magnetic field lines, but the process of wake refilling also occurs across field lines due to the thermal pressure gradient (see Figure 3(2b) and 3(2c)). By this way, the transverse pressure varies, and the field lines will not keep straight but converge towards the center of the wake (Figure 3(2a)). However, the $J \times B$ force produced by field line bending prevents transverse motion, the efficiency of refilling across field lines is lower than that along field lines, and the wake void becomes longer than the case of 90°, as shown in Figure 4(1a) and 4(1b). For the same reason, the effect of adiabatic compression caused by the wake refilling becomes weaker than the 90° case, and thus the temperature increase in the central wake gets smaller (see Figure 4(5a), 4(5b), and 4(5c)). In addition, such deformation of magnetic lines almost causes no force along the *x*-direction to accelerate solar plasma, and there is only a deceleration region in the wake, as shown in Figure 4(4a) and 4(4b). According to the formula in section 2.1, the diamagnetic current at the boundary of the wake is symmetric about the *x*-axis in this case, we can obtain that the magnetic field increases in the central wake, and a cone of lower field strength around the enhanced region (Figure 4(2a), 4(2b) and 4(2c)). In addition, both the field enhancement in the central wake and depression in the expansion region are larger than the case when the IMF and the solar wind velocity are perpendicular, since the magnetic fields and pressure gradients are always close to being perpendicular to each other in the wake and the diamagnetic current is larger on average.

As shown in Figure 4, all the variables are axially symmetrical around the *x*-axis. The Mach cone is circular this time, with a cone angle of about 10° (see Figure 4(1a), 4(2a) and 4(3a)). As discussed in section 2.1, such a cone angle corresponds to the rarefaction wave propagating perpendicular to the magnetic field with the velocity of fast magnetosonic wave.

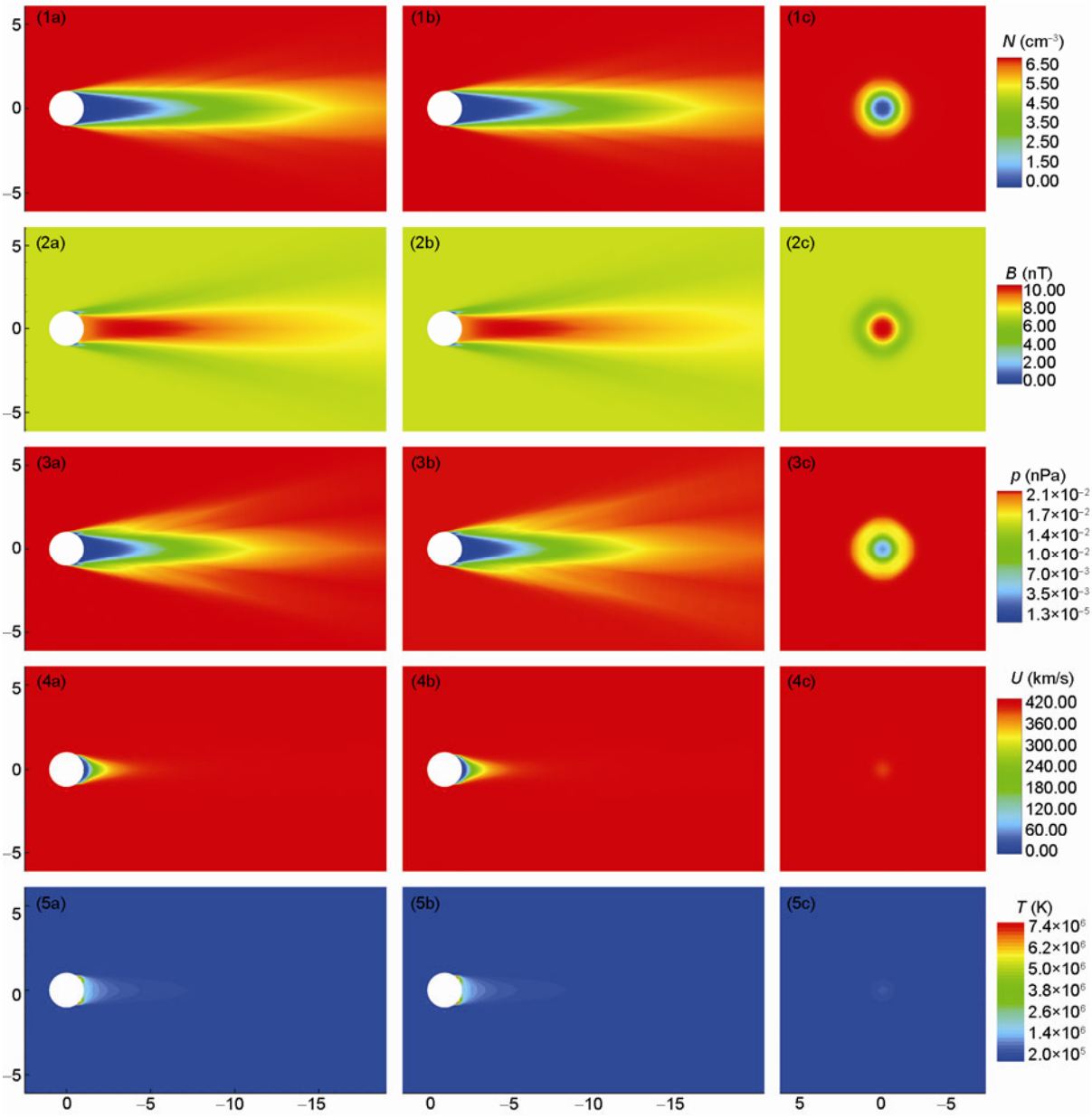

Figure 4 The simulation results for the case of 180°. The columns from left to right are cuts in the planes z=0, y=0 and x=−4R_L. The rows from top to bottom represent the magnitudes of the number density, magnetic field, pressure, velocity and temperature of solar plasma, respectively.

2.3 IMF oblique to the solar wind velocity (135°)

The case of 135° seems to be a mixture of the case of 90° and the case of 180°. Because of the y-component of IMF, the results appear more similar to the case of 90°, such as an acceleration region (see Figure 5(4a) and 5(4b)) in the wake. The field strength in the expansion region is also asymmetric about the x-axis with a larger depression around the polar region. The wake is slightly shorter (Figure 5(1a)) and the magnetic field strength is slightly lower (Figure 5(2b)) than the case of 180°. Nevertheless, there are also some features of the case of 180°, which are chiefly manifested in that the magnetic field seems more symmetric about the x-axis compared with the case of 90° (Figure 5(2c)) and field is also reduced at both sides of the wake in the z=0 plane (Figure 5(2a)). Of course, it has its own specific characteristics, which are reflected in the asymmetry of magnetic field, pressure, and velocity in the y-direction (see Figure 5(2a), 5(3a) and 5(4a)). As shown in Figure 3(3a), bending of magnetic field lines caused by the frozen-in effect also occurs in this case. The difference is that bending does not happen exactly in the x-direction but with an angle to it. Thus the corresponding magnetic force is not directed toward the $-x$-direction but inclines somewhat to the y-direction. Such an inclined force finally causes the asymmetry in the y-direction.

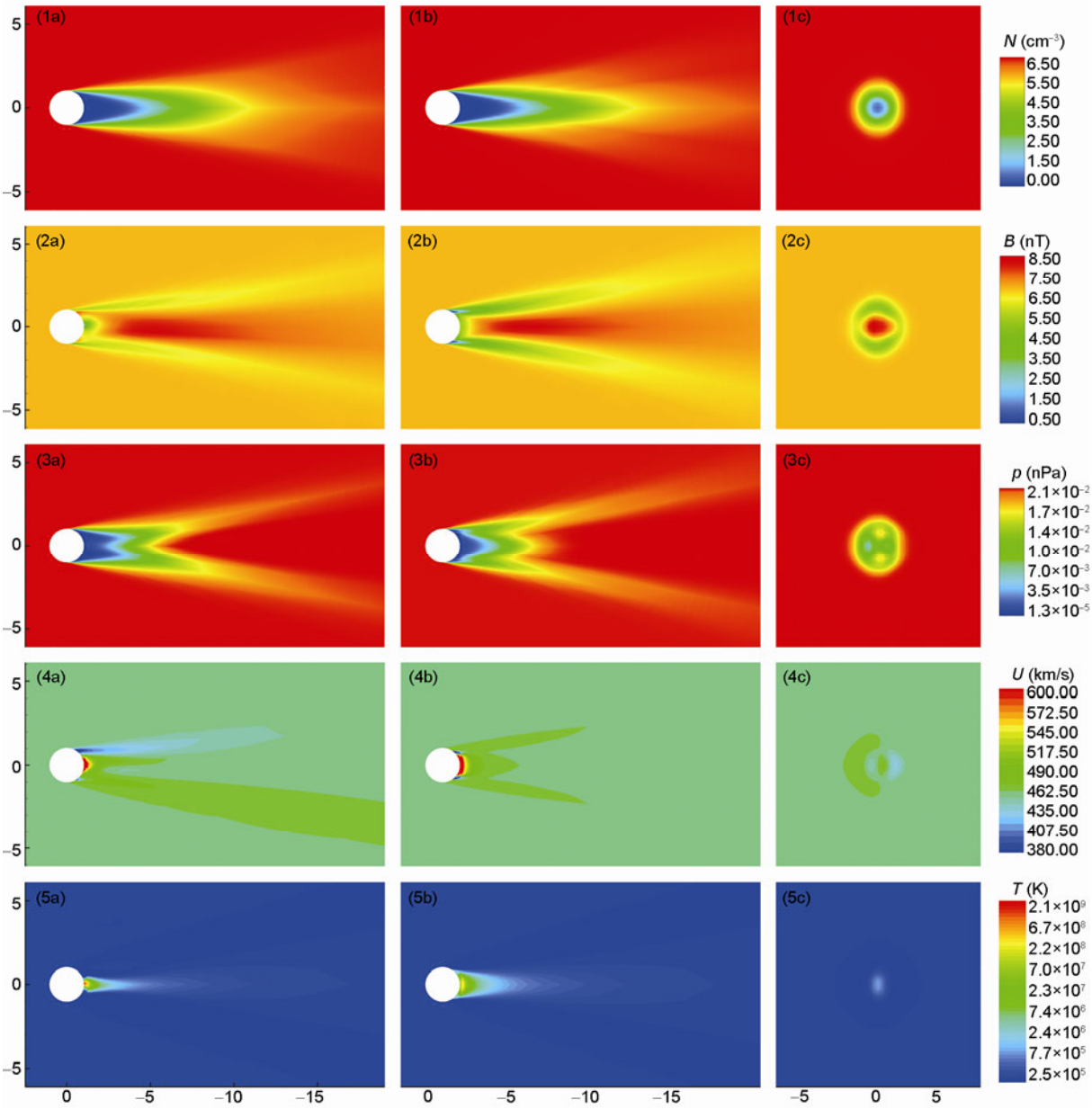

Figure 5 The simulation results for the case of 135°. The columns from left to right are cuts in the planes z=0, y=0 and x=–4R_L. The rows from top to bottom represent the magnitudes of the number density, magnetic field, pressure, velocity and temperature of solar plasma, respectively.

2.4 Comparison with WIND observations

Here we compare the simulation results with the observations by WIND at a distance of x = –6.5R_L from Ogilvie et al. [3]. It should be noted that the solar wind conditions changed during WIND's lunar wake crossing, which is most apparent in the plasma number density that decreases by a factor of two from the undisturbed solar wind on the inbound trajectory to the solar wind on the outbound trajectory. Therefore, as done by Holmström et al. [11], we run the model with two sets of solar wind conditions, and denote them by Before and After, respectively. The solar wind conditions used for Before (After) case are as follows: the velocity is 470 (500) km/s, the number density is 6.0 (2.6) cm^{-3}. The IMF is (5.74, 2.06, 0) nT for Before case, and (5.57, 5.02, 0) nT for After case. The plasma temperature is 2.5×10^5 K for both cases.

As shown in Figure 6, the simulation results match well with the observations by WIND, if we change the comparison from Before case to After case at the center of the wake. We can find, both in the model and in the observations, the plasma number density decreases gradually toward the central wake, the temperature increases by a factor of about four toward the centre of the wake, and the magnetic field strength increases in the central wake but decreases at both sides of the central wake. However, the minimum number

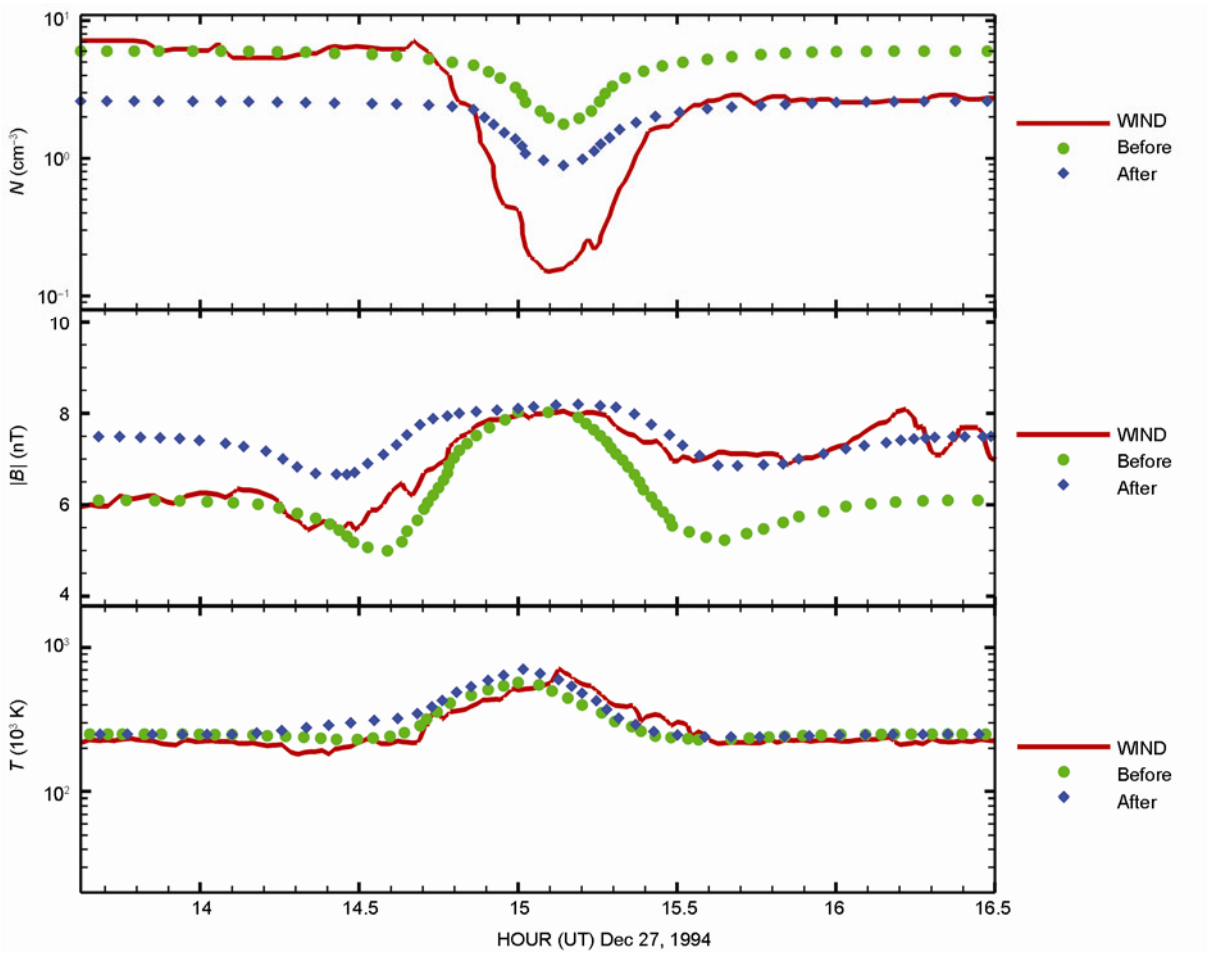

Figure 6 Comparison between simulation results and WIND observations [3]. The rows from top to bottom show the comparison of the plasma number density, magnetic field strength and the temperature, respectively. Here the solid curves represent WIND observations, the dotted curves with circles represent the simulation results for Before case, and the dotted lines with diamonds represent the simulation results for After case.

density of the simulation is much larger than the observed values (see Figure 6), and the lunar wake seems smaller. In reality, the lunar plasma environment is much more complicated than what an MHD model can describe, especially in the region close to the Moon. Particle absorption, reflection and pickup can all happen on the lunar surface according to the observations [18]. In addition, a full description of wake refilling should take into account a number of kinetic effects, such as the ambipolar expansion, instead of a purely magnetosonic expansion. So many mechanisms may make the MHD results deviate from the observation. From the view of MHD simulation, our simplified boundary condition on the night side of the lunar surface might be a reason for the modeled high density in the void. Ions mainly refill the wake along magnetic field lines. Even if the magnetic field is parallel to the solar wind flow, the thermal expansion also allows some ions to enter the lunar wake. In this way, some ions can move towards the lunar surface, part of which can be absorbed. However our MHD model, as a simplified approach, treats the lunar surface as a rigid boundary, and only considers the reflecting effect on the nightside. As a result, the radial velocity equals zero on the lunar surface and all the plasma can bypass the lunar body and flow into the wake without any loss. Such a simplified boundary condition may finally cause the modeled minimum number density larger than the observed values.

3 Conclusions

This paper presents the results from a 3-D global MHD simulation of the interaction between the Moon and the solar wind under three different IMF conditions. Some basic features of the interaction are revealed by this model, including the plasma density decrease in the wake and the central wake magnetic field increase, which are in agreement with the observations [2, 3, 15] and other previous global models [10, 11]. Our model also shows that the plasma temperature is enhanced in the void, and an acceleration region may appear in the near wake. In addition, as the plasma moves into the wake, some rarefaction waves propagate away from the limb via the fast magnetosonic mode,

which is anisotropic and propagates with different velocities in different directions relative to the magnetic field. Our simulation results agree reasonably well with the WIND observations [3]. It should also be admitted that our MHD model also has its limitations for it loses sight of many important mechanisms, such as surface effects, and kinetic processes. In the frame of the MHD method, a Hall MHD model might improve the results in some aspects.

Simulation results were obtained using the Space Weather Modeling Framework, developed by the Center for Space Environment Modeling, at the University of Michigan with funding support from NASA ESS, NASA ESTO-CT, NSF KDI, and DoD MURI. This work was supported by National Natural Science Foundation of China (Grant No. 40974108).

1 Lyon E F, Bridge H S, Binsack J H. Explorer 35 plasma measurements in the vicinity of the Moon. J Geophys Res, 1967, 72: 6113–6117
2 Ness N F, Behannon K W, Taylor H E, et al. Perturbations of the interplanetary magnetic field by the lunar wake. J Geophys Res, 1968, 73: 3421–3440
3 Ogilvie K W, Steinberg J T, Fitzenreiter R J, et al. Observations of the lunar plasma wake from the WIND spacecraft on December 27, 1994. Geophys Res Lett, 1996, 23: 1255–1258
4 Spreiter J R, Marsh M C, Summers A L. Hydromagnetic aspects of solar wind flow past the Moon. Cosm Electrodyn, 1970, 15: 5–50
5 Cui W, Li L. 2D MHD simulation of the lunar wake. Chin J Space Sci, 2008, 28: 189–193
6 Farrell W M, Kaiser M L, Steinberg J T, et al. A simple simulation of a plasma void: Applications to Wind observations of the lunar wake. J Geophys Res, 1998, 103: 23653–23660
7 Birch P C, Chapman S C. Particle-in-cell simulations of the lunar wake with high phase space resolution. Geophys Res Lett, 2001, 28: 219–222
8 Birch P C, Chapman S C. Two dimensional particle-in-cell simulations of the lunar wake. Phys Plasmas, 2002, 9: 1785–1789
9 Trávníček P, Hellinger P, Schriver D, et al. Structure of the lunar wake: Two-dimensional global hybrid simulations. Geophys Res Lett, 2005, 32: L06102, doi: 10.1029/2004GL022243
10 Kallio E. Formation of the lunar wake in quasi-neutral hybrid model. Geophys Res Lett, 2005, 32: L06107, doi: 10.1029/2004GL021989
11 Holmström M, Fatemi S, Futaana Y, et al. The interaction between the Moon and the solar wind. Earth Planets Space, 2012, 64: 237–245
12 Tóth G, Holst B V D, Sokolov I V, et al. Adaptive numerical algorithms in space weather modeling. J Computation Phys, 2012, 231: 870–903, doi: 10.1016/j.jcp.2011.02.006
13 Linde T J. A three-dimensional adaptive multifiuid MHD model of the heliosphere. PhD Thesis. Ann Arbor: University of Michigan, 1998
14 Kivelson M G, Russell C T. Introduction to Space Physics. Cambridge: Cambridge University Press, 1995
15 Halekas J S, Bale S D, Mitchell D L, et al. Electrons and magnetic fields in the lunar plasma wake. J Geophys Res, 2005, 110: A07222, doi: 10.1029/2004JA010991
16 Colburn D S, Currie R G, Mihalov J D, et al. Diamagnetic solar-wind cavity discovered behind moon. Science, 1967, 158: 1040–1042
17 Colburn D S, Mihalov J D, Sonett C P. Magnetic observations of the lunar cavity. J Geophys Res, 1971, 76: 2940–2957
18 Halekas J S, Saito Y, Delory G T, et al. New views of the lunar plasma environment. Planet Space Sci, 2011, 59: 1681–1694, doi: 10.1016/j.pss.2010.08.011